

Supplementary information for

## **Faceted and defect-rich $\text{CuMn}_2\text{O}_4$ nanoparticles for efficient electrochemical water splitting**

*Balasubramanian Jansi Rani<sup>a,b,†</sup>, Arumugam Sivanantham<sup>a,c,†</sup>, Tatachari Santhanagopalan Shridharan<sup>a,c</sup>, Tan Runfa<sup>a,c</sup>, and In Sun Cho<sup>a,c,\*</sup>*

<sup>a</sup> Department of Materials Science & Engineering, Ajou University, Suwon 16499, South Korea

<sup>b</sup> Engineering Research Institute, Ajou University, Suwon 16499, South Korea

<sup>c</sup> Department of Energy Systems Research, Ajou University, Suwon 16499, South Korea

† These authors contributed equally to this work.

\*Corresponding Author email: [insuncho@ajou.ac.kr](mailto:insuncho@ajou.ac.kr) (I.S.C)

## Experimental section

### *Deposition of CoO<sub>x</sub> nanoparticles on f-CMO-600 electrode*

CoO<sub>x</sub> coating solution (0.5 M) was prepared by the sol-gel method. Briefly, 0.5 mmol of Co(NO<sub>3</sub>)<sub>2</sub>·6H<sub>2</sub>O (0.146 g) was dissolved in 10 mL of 2-methoxyethanol (2-ME) and sonicated for 30 min to get a transparent pink color solution. Then f-CMO-600 coated Cu foam substrate was dip-coated with the prepared 0.5 M CoO<sub>x</sub> solution for 30 s, followed by 350 °C thermal annealing for 30 min to obtain CoO<sub>x</sub>/f-CMO-600 electrode. All the electrodes were finally subjected to UV epoxy to avoid the electrolyte uplifting through the Cu foam handles during the experiments.

### *Preparation of f-CMO pellets for Hall voltage measurements*

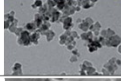
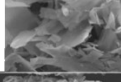
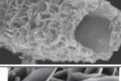
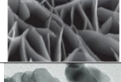
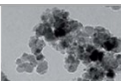
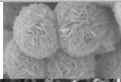
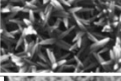

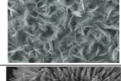


The grounded f-CMO powders were pressed (without a binder) into a pellet (Ø = 15 mm, height = 2 mm) with a hydraulic press (DAEWHA, P-50t, South Korea) at a pressure of 900 MPa for 10 s and Zn-stearate was used as a lubricant to prevent fracturing at the die-wall.

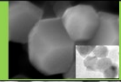

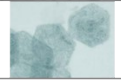
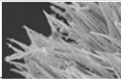
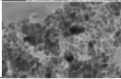
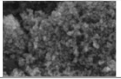
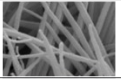
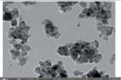
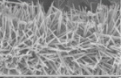
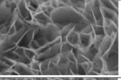
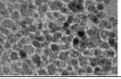
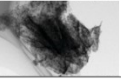
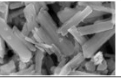
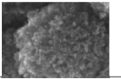

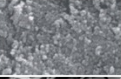
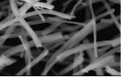
**Table S1.** Inductively coupled plasma-optical emission spectrometry (ICP-OES) result of the f-CMO-600 sample.

<b>Elements</b>	<i>ppb</i>	<i>Mole</i>
<i>Cu</i>	248270.250	1.04
<i>Mn</i>	460131.093	1.93

Thus, the metal molar ratio is Cu: Mn = 1: 1.86.

**Table S2.** Comparison of electrocatalytic HER activity of faceted CuMn<sub>2</sub>O<sub>4</sub> nanoparticles (f-CMO) with other reported spinel oxides.

Family	Electrocatalyst materials	Morphology	SEM/TEM image	Electrolyte	HER Overpotential @-100 mA/cm <sup>2</sup> (mV vs. RHE)	Ref.
Spinel oxides	f-CuMn <sub>2</sub> O <sub>4</sub>	Nanopolyhedra		1 M KOH	234	This work
	NiFe <sub>2</sub> O <sub>4</sub>	Nanoparticles		1 M KOH	241 @-80 mA/cm <sup>2</sup>	[1]
	NiCo <sub>2</sub> O <sub>4</sub>	Nanosheets		1 M KOH	255 @-60 mA/cm <sup>2</sup>	[2]
	NiCo <sub>2</sub> O <sub>4</sub>	Hollow microcuboids		0.5 M H <sub>2</sub> SO <sub>4</sub>	265	[3]
	NiCo <sub>2</sub> O <sub>4</sub>	Nanosheets		1 M KOH	272	[4]
	CoMn <sub>2</sub> O <sub>4</sub>	3D tetragons		0.1 M KOH	284	[5]
	Co <sub>3</sub> O <sub>4</sub>	Hollow microtube arrays		1 M KOH	291	[6]
	Fe <sub>3</sub> O <sub>4</sub>	-	-	6 M KOH	305	[7]
	CoFe <sub>2</sub> O <sub>4</sub>	Nanoparticles		1 M KOH	314 @-80 mA/cm <sup>2</sup>	[1]
	CoMn <sub>2</sub> O <sub>4</sub>	Nanoflowers		1 M KOH	320	[8]
	NiCo <sub>2</sub> O <sub>4</sub>	Nanowire arrays		1 M KOH	321	[9]
	CoCr <sub>2</sub> O <sub>4</sub>	Mesoporous nanocast		1 M KOH	342	[10]
	CoMn <sub>2</sub> O <sub>4</sub>	Nanoflake arrays		1 M NaOH	348	[11]
	NiCo <sub>2</sub> O <sub>4</sub>	Urchin like peapods		1 M NaOH	349	[12]
	CoFe <sub>2</sub> O <sub>4</sub>	-	-	1 M NaOH	352	[13]
	NiCo <sub>2</sub> O <sub>4</sub>	Porous nanowires		1 M KOH	358	[14]
	NiCo <sub>2</sub> O <sub>4</sub>	Mesoporous nanoarrays		1 M KOH	363	[15]

Family	Electrocatalyst materials	Morphology	SEM/TEM image	Electrolyte	HER Overpotential @-100 mA/cm <sup>2</sup> (mV vs. RHE)	Ref.
Spinel oxides	f-CuMn <sub>2</sub> O <sub>4</sub>	Nanopolyhedra		1 M KOH	234	This work
	NiCo <sub>2</sub> O <sub>4</sub>	Nanoneedle arrays		4 M KOH	378	[16]
	NiCo <sub>2</sub> O <sub>4</sub>	Nanosheets		1 M KOH	379 @-20 mA/cm <sup>2</sup>	[17]
	MnCo <sub>2</sub> O <sub>4</sub>	Hierarchical arrays		1 M KOH	385	[18]
	NiFe <sub>2</sub> O <sub>4</sub>	Nanoparticles		0.5 M H <sub>2</sub> SO <sub>4</sub>	405	[19]
	NiFe <sub>2</sub> O <sub>4</sub>	Nanoparticles		0.5 M KOH	420	[20]
	NiCo <sub>2</sub> O <sub>4</sub>	Nanowires		6 M KOH	421	[21]
	ZnFe <sub>2</sub> O <sub>4</sub>	Nanoparticles		1 M KOH	432 @-80 mA/cm <sup>2</sup>	[1]
	MnCo <sub>2</sub> O <sub>4</sub>	1D nanowires		1 M KOH	446	[22]
	NiCo <sub>2</sub> O <sub>4</sub>	Nanoflakes		1 M KOH	469	[23]
	NiFe <sub>2</sub> O <sub>4</sub>	Nanoparticles		1 M KOH	487	[24]
	Co <sub>3</sub> O <sub>4</sub>	Nanosheet arrays		1 M KOH	513	[25]
	MnCo <sub>2</sub> O <sub>4</sub>	Microrods		1 M KOH	600 @-20 mA/cm <sup>2</sup>	[26]
	Co <sub>3</sub> O <sub>4</sub>	Florets		1 M KOH	646	[27]
	Co <sub>3</sub> O <sub>4</sub>	Nanoparticles aggregated hexagonal flakes		1 M KOH	646 @-60 mA/cm <sup>2</sup>	[28]
	NiFe <sub>2</sub> O <sub>4</sub>	Nanoparticles		0.5 M KOH	676	[29]
	MnCo <sub>2</sub> O <sub>4</sub>	Nanofibers		1 M KOH	677 @-10 mA/cm <sup>2</sup>	[30]

## References

- (1) C. Fan, X. Zhai, L. Chen, S. Peng, R. Jiang, J. Yu, Y. Li, Y. Zhang, W. Kong, G. Ge and X. Guo, *J. Mater. Chem. A*, 2021, **9**, 22277–22290.
- (2) L. Fang, Z. Jiang, H. Xu, L. Liu, Y. guan, X. Gu and Y. Wang, *J. Catal.*, 2018, **357**, 238–246.
- (3) X. Gao, H. Zhang, Q. Li, X. Yu, Z. Hong, X. Zhang, C. Liang and Z. Lin, *Angew. Chemie - Int. Ed.*, 2016, **55**, 6290–6294.
- (4) C. Xiao, Y. Li, X. Lu and C. Zhao, *Adv. Funct. Mater.*, 2016, **26**, 3515–3523.
- (5) G. Janani, S. Surendran, H. Choi, M. K. Han and U. Sim, *Small*, 2021, **17**, 1–16.
- (6) Y. P. Zhu, T. Y. Ma, M. Jaroniec and S. Z. Qiao, *Angew. Chemie - Int. Ed.*, 2017, **56**, 1324–1328.
- (7) J. Zhang, X. Shang, H. Ren, J. Chi, H. Fu, B. Dong, C. Liu and Y. Chai, *Adv. Mater.*, 2019, **31**, 1–10.
- (8) J. Lee, N. Son, N. K. Park, H. J. Ryu, J. I. Baek, Y. Sohn, J. Y. Do and M. Kang, *Electrochim. Acta*, 2021, **379**, 138168.
- (9) B. Wei, J. Wu, G. Mei, Z. Qi, W. Hu and Z. Wang, *Int. J. Hydrogen Energy*, 2019, **44**, 6612–6617.
- (10) A. Saad, H. Shen, Z. Cheng, Q. Ju, H. Guo, M. Munir, A. Turak, J. Wang and M. Yang, *ACS Appl. Energy Mater.*, 2020, **3**, 1684–1693.
- (11) C. Wang, H. Lu, Z. Mao, C. Yan, G. Shen and X. Wang, *Adv. Funct. Mater.*, 2020, **30**, 1–10.
- (12) J. Deng, H. Zhang, Y. Zhang, P. Luo, L. Liu and Y. Wang, *J. Power Sources*, 2017, **372**, 46–53.
- (13) H. Zhang, G. Qian, X. Chen, W. Jiang, T. Yu, Y. Wang, L. Luo and S. Yin, *ACS Sustain. Chem. Eng.*, 2021, **9**, 980–986.
- (14) Y. Ha, L. Shi, X. Yan, Z. Chen, Y. Li, W. Xu and R. Wu, *ACS Appl. Mater. Interfaces*, 2019, **11**, 45546–45553.
- (15) D. Liu, C. Zhang, Y. Yu, Y. Shi, Y. Yu, Z. Niu and B. Zhang, *Nano Res.*, 2018, **11**, 603–613.
- (16) T. Liu and P. Diao, *Nano Res.*, 2020, **13**, 3299–3309.
- (17) F. Lai, J. Feng, X. Ye, W. Zong, G. He, Y. E. Miao, X. Han, X. Y. Ling, I. P. Parkin, B. Pan, Y. Sun and T. Liu, *J. Mater. Chem. A*, 2019, **7**, 827–833.
- (18) J. Ge, W. Zhang, J. Tu, T. Xia, S. Chen and G. Xie, *Small*, 2020, **16**, 1–9.
- (19) A. Mukherjee, S. Chakrabarty, W. N. Su and S. Basu, *Mater. Today Energy*, 2018, **8**, 118–124.
- (20) P. V. Shinde, P. Mane, B. Chakraborty and C. Sekhar Rout, *J. Colloid Interface Sci.*, 2021, **602**, 232–241.
- (21) W. Chu, Z. Shi, Y. Hou, D. Ma, X. Bai, Y. Gao and N. Yang, *ACS Appl. Mater. Interfaces*, 2020, **12**, 2763–2772.
- (22) L. Qi, Z. Zheng, C. Xing, Z. Wang, X. Luan, Y. Xue, F. He and Y. Li, *Adv. Funct. Mater.*, 2021, **2107179**, 1–9.
- (23) Z. Liu, H. Tan, D. Liu, X. Liu, J. Xin, J. Xie, M. Zhao, L. Song, L. Dai and H. Liu, *Adv. Sci.*, , DOI:10.1002/advs.201801829.
- (24) J. Jin, J. Yin, H. Liu, B. Huang, Y. Hu, H. Zhang, M. Sun, Y. Peng, P. Xi and C. Yan,

- Angew. Chemie*, 2021, **133**, 14236–14242.
- (25) Z. Xiao, Y. Wang, Y. C. Huang, Z. Wei, C. L. Dong, J. Ma, S. Shen, Y. Li and S. Wang, *Energy Environ. Sci.*, 2017, **10**, 2563–2569.
- (26) X. Huang, H. Zheng, G. Lu, P. Wang, L. Xing, J. Wang and G. Wang, *ACS Sustain. Chem. Eng.*, 2019, **7**, 1169–1177.
- (27) J. Saha, R. Ball, A. Sah, V. Kalyani and C. Subramaniam, *Nanoscale*, 2019, **11**, 13532–13540.
- (28) X. Zhao, F. Yin, X. He, B. Chen and G. Li, *Electrochim. Acta*, 2020, **363**, 137230.
- (29) P. V. Shinde, S. Babu, S. K. Mishra, D. Late, C. S. Rout and M. K. Singh, *Sustain. Energy Fuels*, 2021, **5**, 3906–3917.
- (30) C. Wu, C. Li, B. Yang, S. Zhou, D. Shi, Y. Wang, G. Yang and J. He, *Mat. Res. Express*, 2016, **3**, 095018.

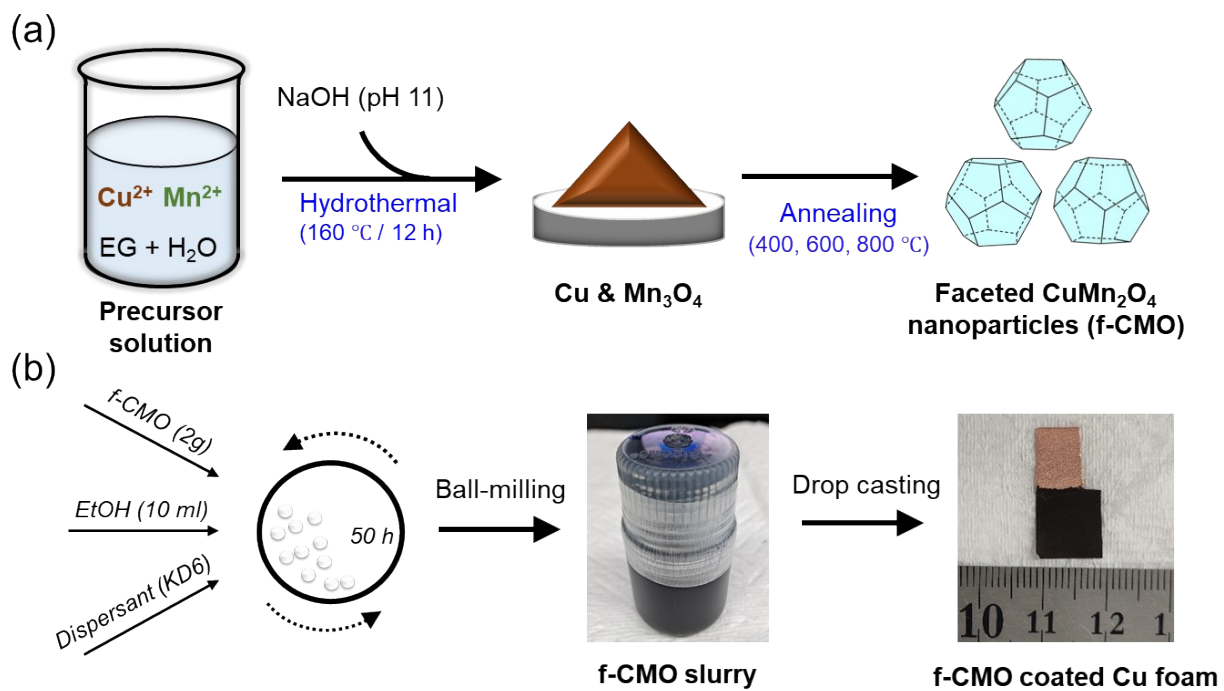
**Table S3.** Summary of electrochemical impedance spectra (EIS) fitting:  $R_1$ ,  $R_2$  and  $R_3$  (applied bias: -0.1 V vs. RHE; Frequency range: 7 MHz to 1 mHz).

<b>Electrode</b>	$R_1$ (Ohm)	$R_2$ (Ohm)	$R_3$ (Ohm)
<i>f</i> -CMO-400	1.9	3.1	64.1
<i>f</i> -CMO-600	1.8	1.5	56.0
<i>f</i> -CMO-800	1.8	2.8	57.7

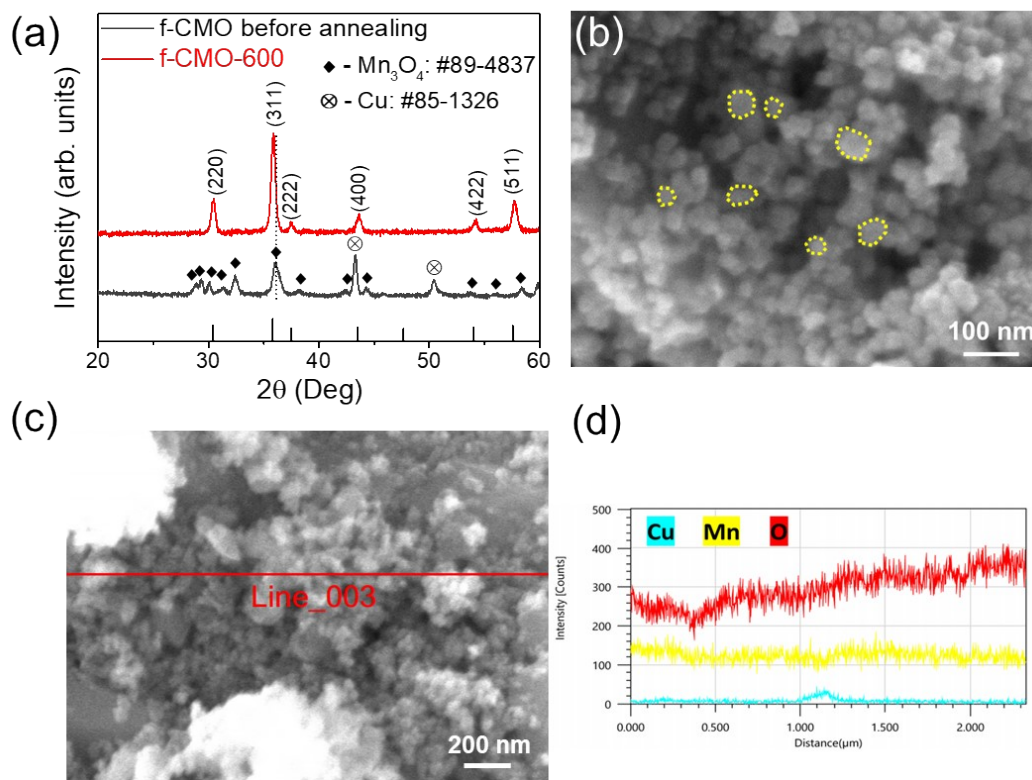
**Table S4.** Summary of electrochemical impedance spectra (EIS) fitting:  $R_1$ ,  $R_2$  and  $R_3$  (applied bias: 1.6 V vs. RHE; Frequency range: 7 MHz to 1 mHz).

<b>Electrode`</b>	$R_1$ (Ohm)	$R_2$ (Ohm)	$R_3$ (Ohm)
<i>f</i> -CMO-400	2.0	2.2	10.2
<i>f</i> -CMO-600	2.0	2.0	4.0
<i>f</i> -CMO-800	1.9	2.3	4.5
CoO <sub>x</sub> / <i>f</i> -CMO-600	2.1	1.9	3.7

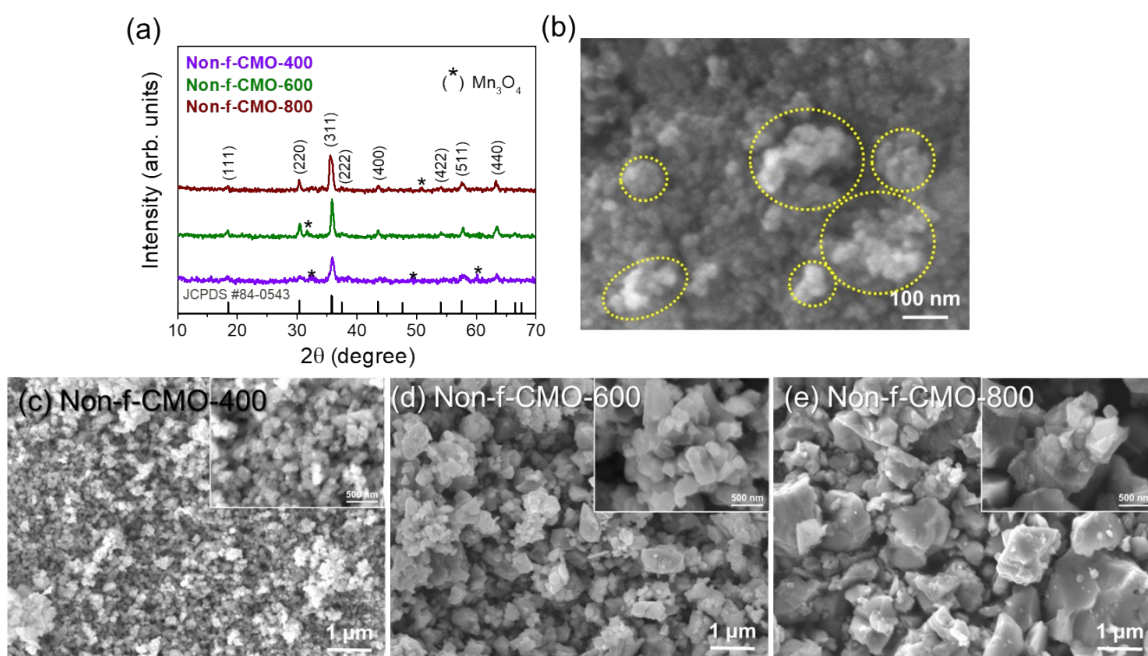




**Fig. S1. Synthesis and slurry preparation of faceted  $\text{CuMn}_2\text{O}_4$  nanoparticles (f-CMO):** (a) Synthesis scheme. (b) Slurry preparation *via* ball milling.

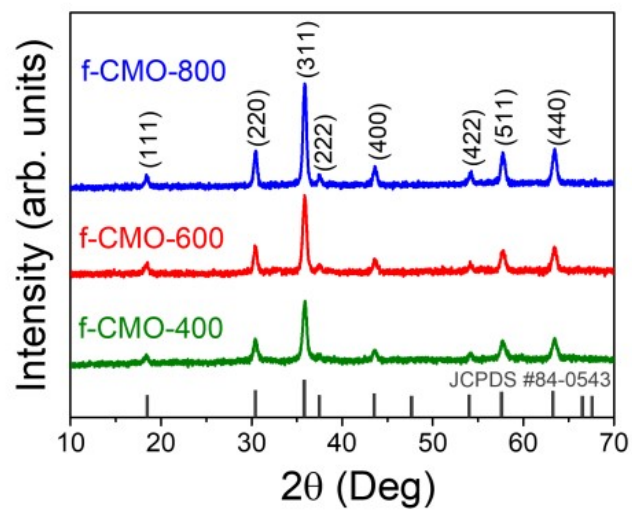


**Fig. S2. Structural and morphological analyses:** (a) XRD pattern of f-CMO before and after annealing at 600 °C. (b) SEM image of f-CMO before annealing. (c,d) SEM-EDS line scan spectrum of f-CMO before annealing.

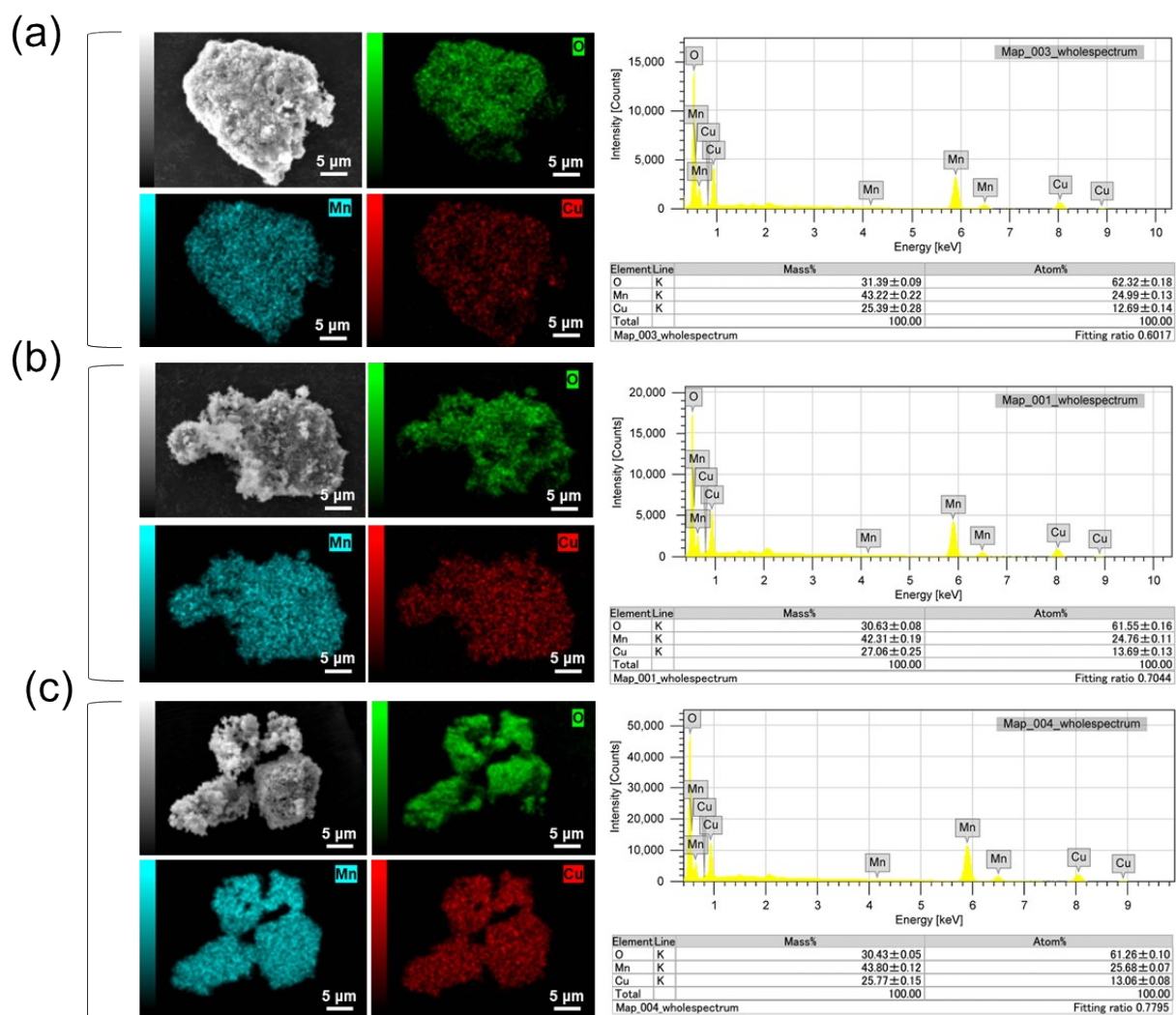


**Fig. S3. Structural and morphological analyses of non-f-CMOs:** (a) XRD pattern. SEM images of (b) before annealing, and (c-e) after annealing.

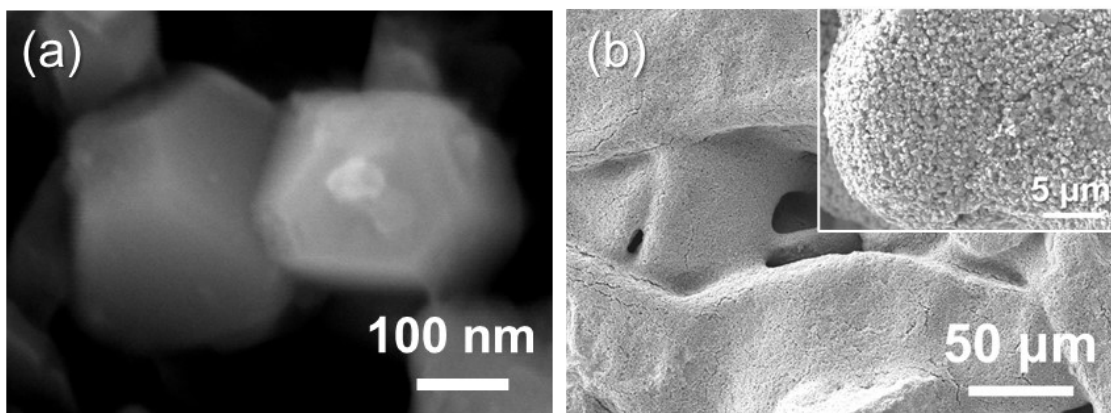
Further, to examine the role of the hydrothermal treatment (HT) on the facet formation, CMO has been synthesized by using only co-precipitation (without HT) and named as non-f-CMO, as illustrated in **Fig. S3**. Here, the formation of the non-f-CMO was confirmed by the crystal planes such as (111), (220), (311), (222), (400), (422), (511), and (440), which correspond to the cubic crystal structure of CMO (JCPDS #84-0543), with some  $\text{Mn}_3\text{O}_4$  impurities (**Fig. S3a**). Thus, the synthesis condition without HT had a negative influence on the formation of phase-pure CMO. Moreover, the larger aggregation of undefined nanoparticles (before annealing) resulted from the uncontrolled growth (**Fig. S3b**). After annealing, the size of non-f-CMOs are almost ten times greater than f-CMO (**Fig. S3c-e**). Therefore, this result confirms that co-precipitation without a controlled atmosphere (optimum HT temperature and reaction time) fails to produce the phase-pure and size-controlled f-CMO.



**Fig. S4.** X-ray diffraction (XRD) patterns of the f-CMO-400, f-CMO-600 and f-CMO-800.



**Fig. S5. Elemental mapping and EDX spectral analysis of f-CMO: (a) f-CMO-400. (b) f-CMO-600. (c) f-CMO-800.**

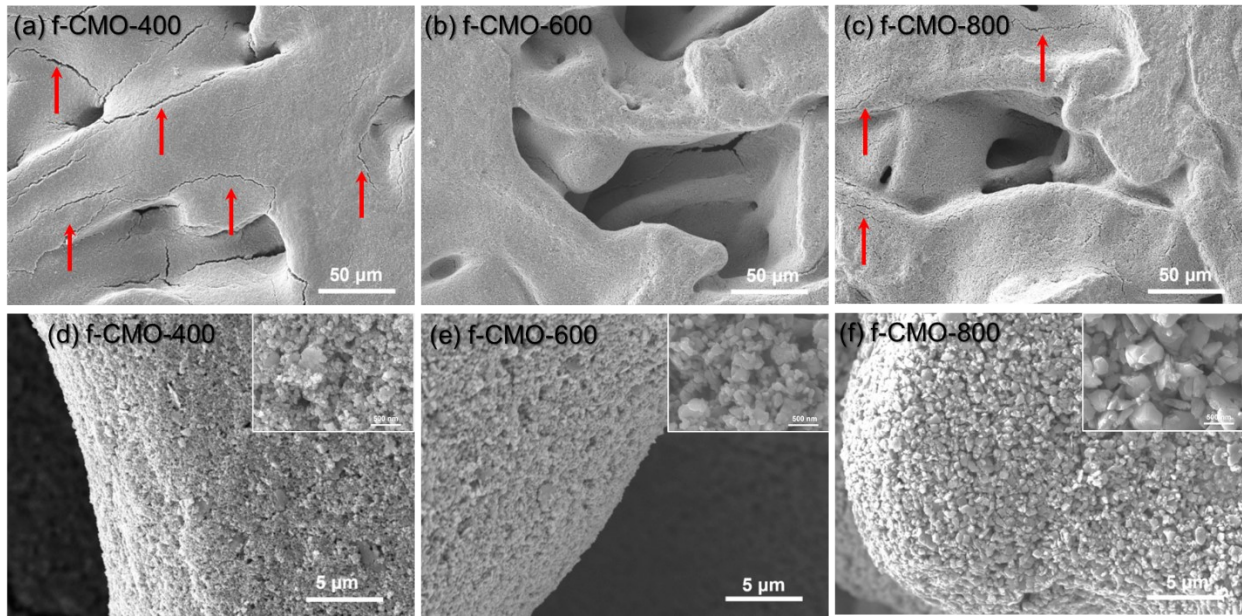


**Fig. S6.** Scanning electron microscope (SEM) images of (a) f-CMO-800 slurry after 50 h ball milling. (b) f-CMO-800 electrode.

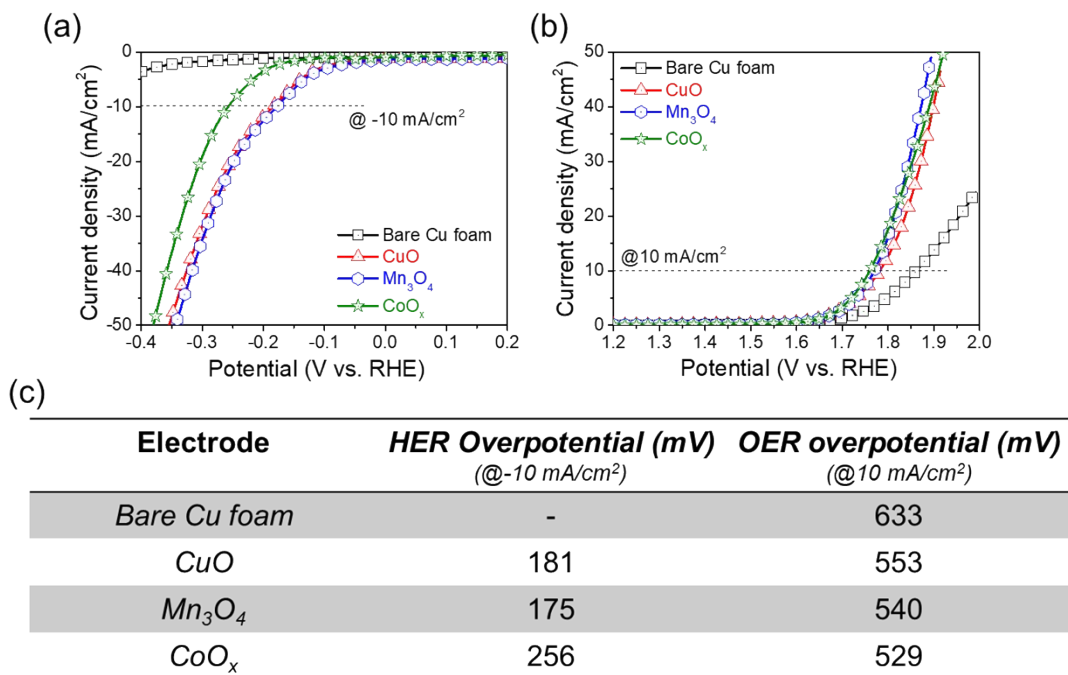
The SEM analysis of f-CMO-800 catalyst after the 50 h ball milling process was performed to check the structure changes. Notably, even after the long-term ball milling, the structure of the catalyst exhibits the same faceted morphology without any noticeable changes, confirming the structure stability of f-CMO. Our intention to use the ball milling to prepare electrodes was the employment of an inexpensive, facile and scalable method to obtain a well-dispersed and high-quality slurry for the conformal coating of catalyst on the substrate<sup>1</sup>.

**Reference:**

1. A. Kraytsberg, and Y. Ein-Eli, *Adv. Energy Mater.*, 2016, **6**, 1600655.

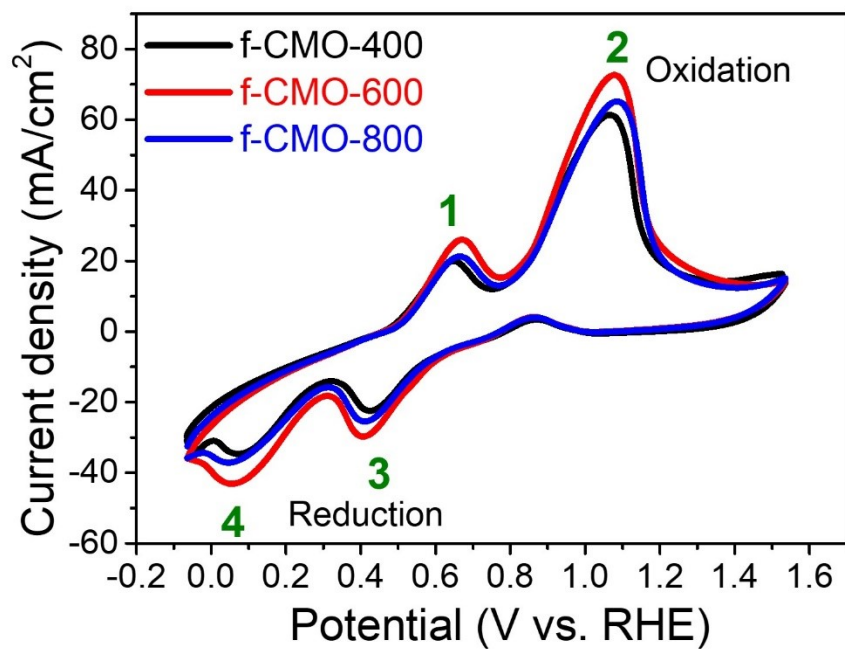


**Fig. S7. Surface analysis of f-CMO electrodes: SEM images.** (a-c) Low magnification. (d-f) High magnification (image insets are at 500 nm). Red color arrow points out the cracks on the f-CMO electrode surface.

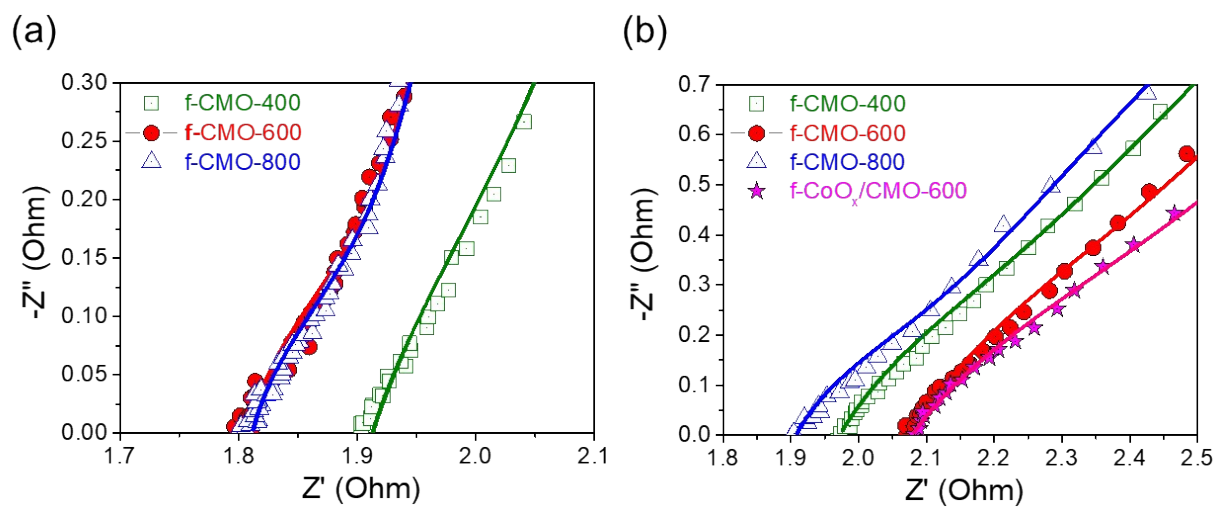


**Fig. S8. Linear sweep voltammograms (LSVs) of the control samples: (a) HER. (b) OER. (c) Comparison of the overpotential values.**

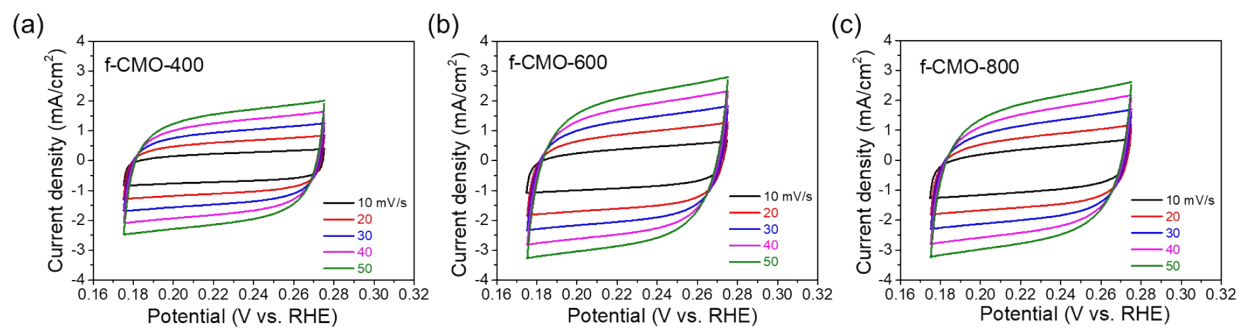




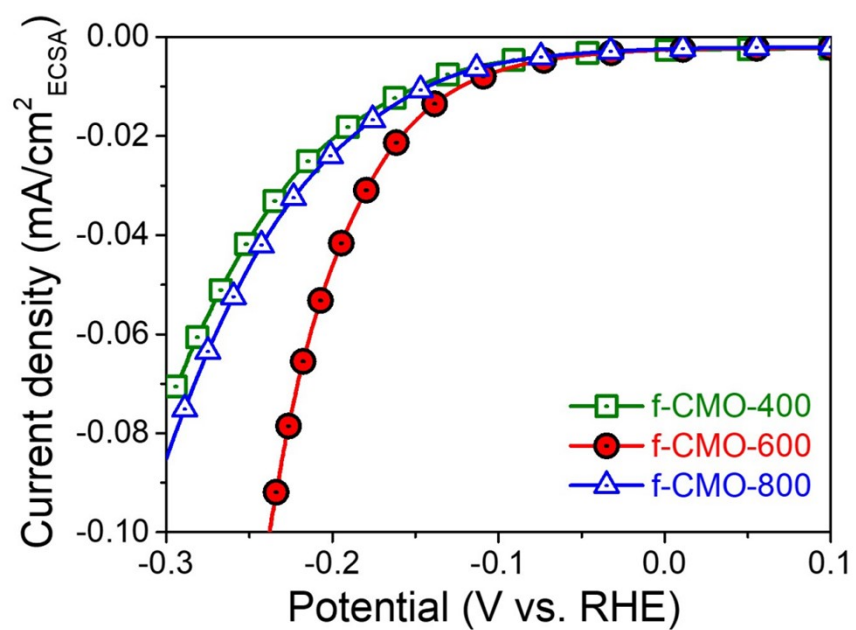
**Fig. S9.** Redox behavior of f-CMO electrodes *via* cyclic voltammograms (CVs) at 5 mV/s in 1 M KOH alkaline electrolyte.



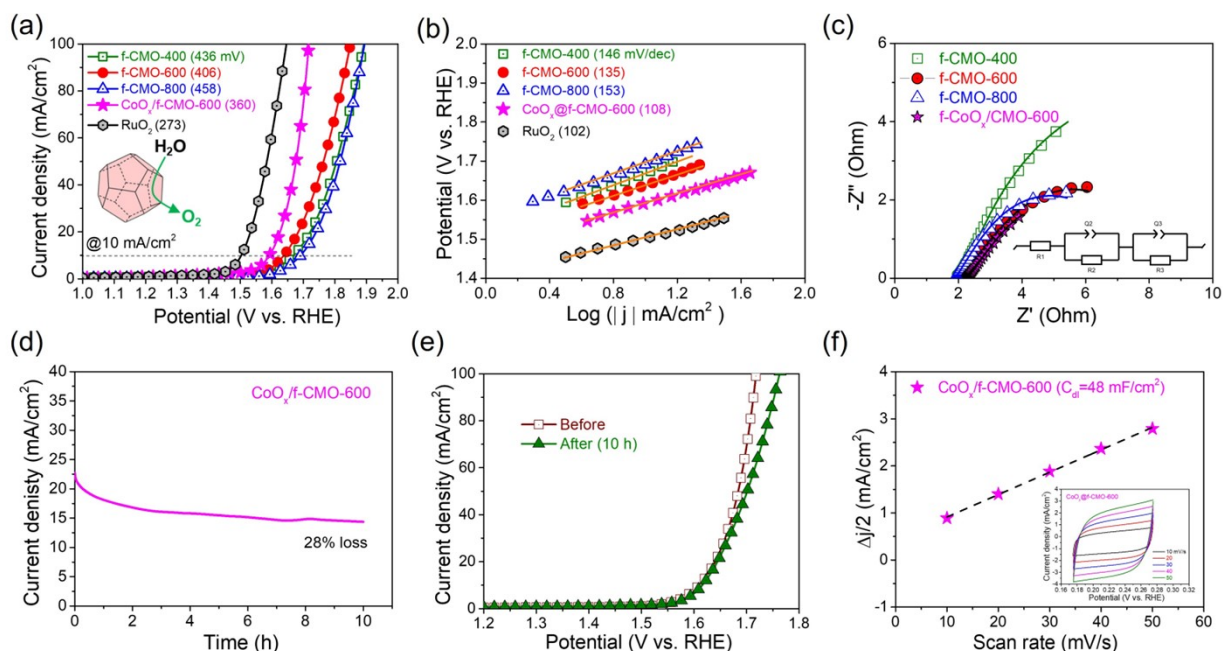
**Fig. S10.** Zoom-in EIS spectra of the f-CMO electrodes, obtained at (a)  $-0.1$  V vs. RHE. (b)  $1.6$  V vs. RHE.



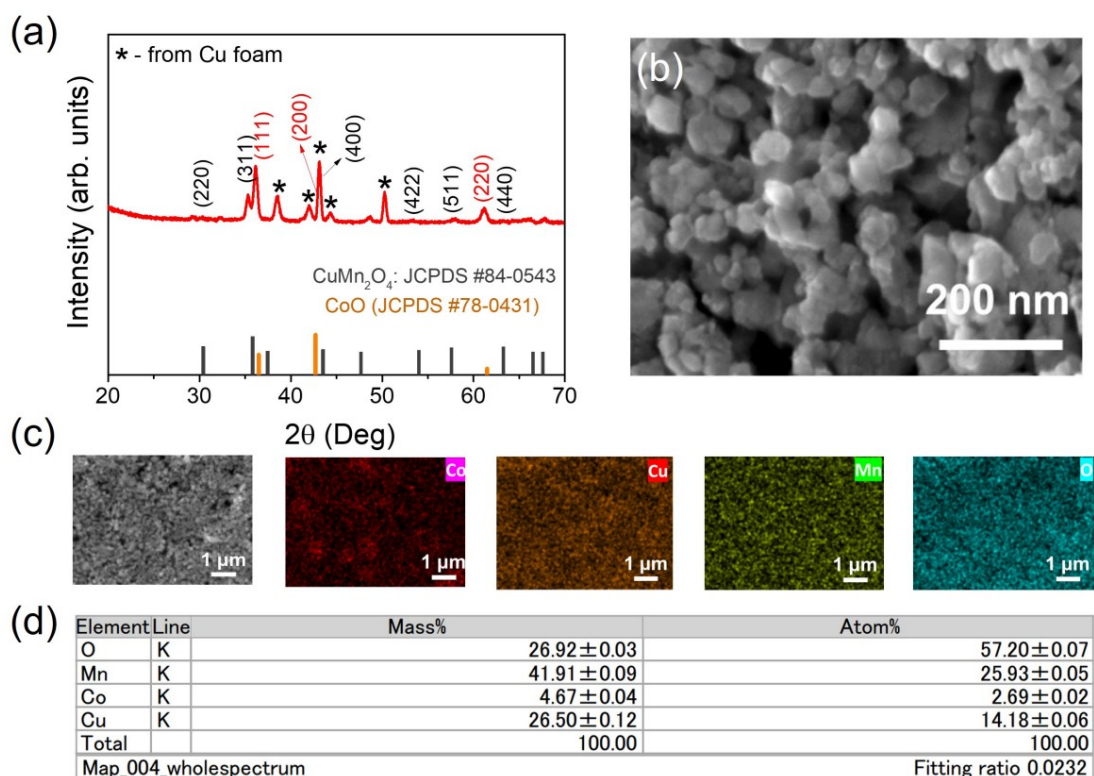
**Fig. S11. Electrochemical active surface area analysis of f-CMO electrodes:** Cyclic voltammograms (CVs) of (a) f-CMO-400. (b) f-CMO-600. (c) f-CMO-800 at different scan rates (10, 20, 30, 40 and 50 mV/s).



**Fig. S12. Intrinsic catalytic activity:** Linear sweep voltammograms (current density) of f-CMO electrodes normalized by ECSA.



**Fig. S13. Electrocatalytic OER activity of f-CMO and CoO<sub>x</sub>/f-CMO-600 electrodes for water splitting in 1 M KOH:** (a) Linear sweep voltammograms (LSVs). (b) Corresponding Tafel plots. (c) Nyquist plot at 1.6 V vs. RHE. (d) Chronoamperometry (CA) stability test of f-CMO-600 at 1.665 V vs. RHE for 10 h. (e) Linear sweep voltammogram (LSV) before and after stability. (f) Electrochemical surface area (ECSA), and cyclic voltammogram (CV) of CoO<sub>x</sub>/f-CMO-600 (inset image).

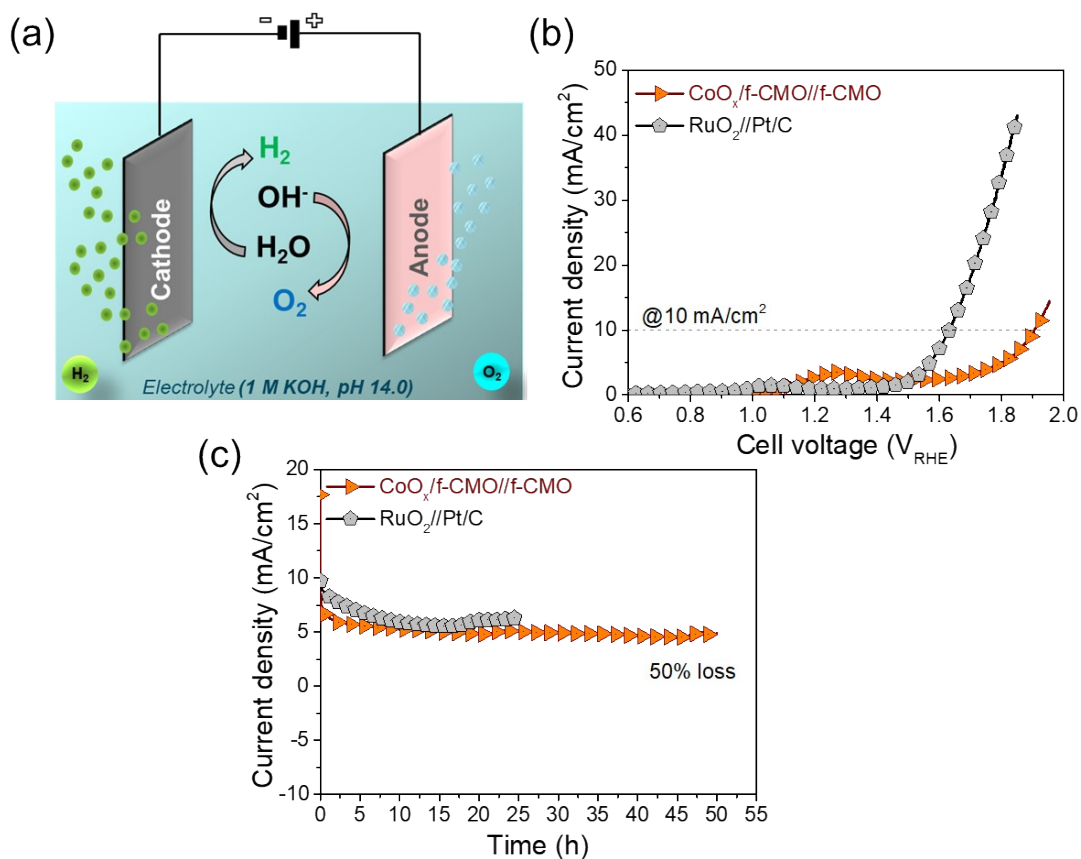


**Fig. S14. Structural and morphological analyses of CoO<sub>x</sub>/f-CMO-600 electrode:** (a) XRD pattern. (b) SEM image. (c) SEM-EDS elemental mapping. (d) SEM-EDS microanalysis results.

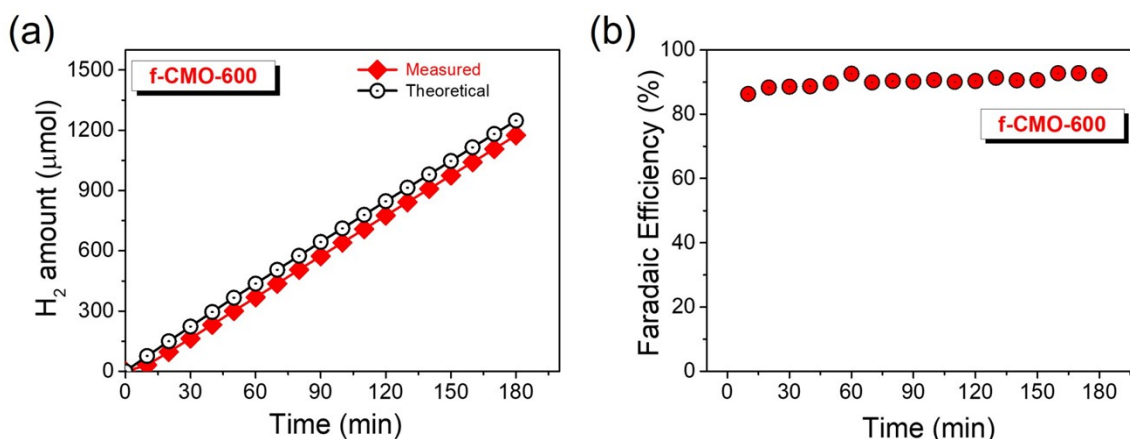
The XRD, SEM and EDS mapping results of the CoO<sub>x</sub>/f-CMO-600 electrode are given **Fig. S14**. The XRD result (**Fig. S14a**) confirms the formation of the CoO<sub>x</sub> coating from the diffraction peaks of the crystal planes (111), (200) and (220), which coincide with hexagonal CoO (JCPDS #78-0421)<sup>2</sup>. The SEM image (**Fig. S14b**) shows the faceted morphology of the CoO<sub>x</sub>/f-CMO-600 electrode. Furthermore, **Fig. S14c,d** shows uniform distribution and existence of Co, Cu, Mn and O in the CoO<sub>x</sub>/f-CMO-600. Therefore, the formation of CoO<sub>x</sub> coated f-CMO-600 is confirmed from XRD, SEM and EDS results.

## Reference

2. K. Deori, and S. Deka, *Cryst Eng Comm.*, 2013, **15**, 8465-8474.



**Fig. S15. Electrochemical performance of the two-electrode cell for overall water splitting:** (a) Schematic representation of two-electrode cell. (b) Linear sweep voltammograms (LSVs). (c) Chronoamperometry (CA) at a cell voltage of 1.90 and 1.65 V for  $\text{CoO}_x/\text{f-CMO}/\text{f-CMO}$  and  $\text{RuO}_2/\text{Pt/C}$  respectively, in 1 M KOH.



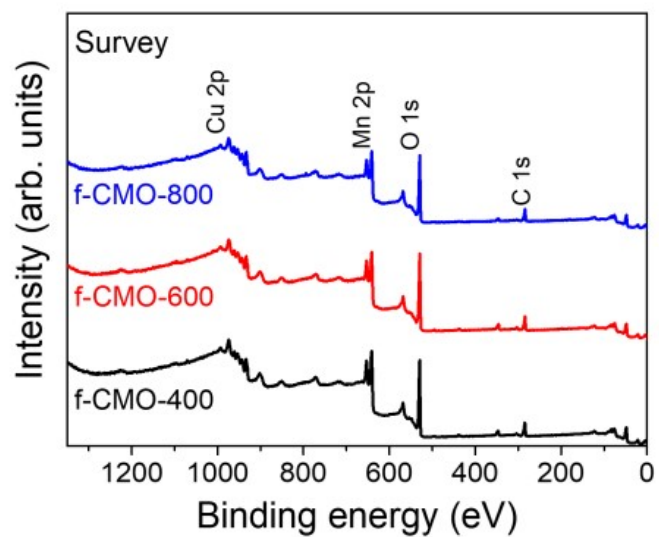
**Fig. S16. Gas-product collected after HER activity for 3 h (at -0.283 V vs. RHE) of f-CMO-600 electrode: (a) H<sub>2</sub> evolution. (b) Faradaic efficiency (%).**

The hydrogen evolution was measured by using a gas chromatograph (YL6500GC, Young In Chromass, South Korea) connected with a pulsed discharge detector (PDD) and a 5 Å zeolite molecular sieve column, from the chronoamperometry test (at -0.283 V vs. RHE) for 3 h. Initially, the electrolyte was adequately purged with helium (He) gas to remove residual gases from the electrochemical cell. Faradaic efficiency (FE) was calculated (**Fig. S16**) using the following equation:

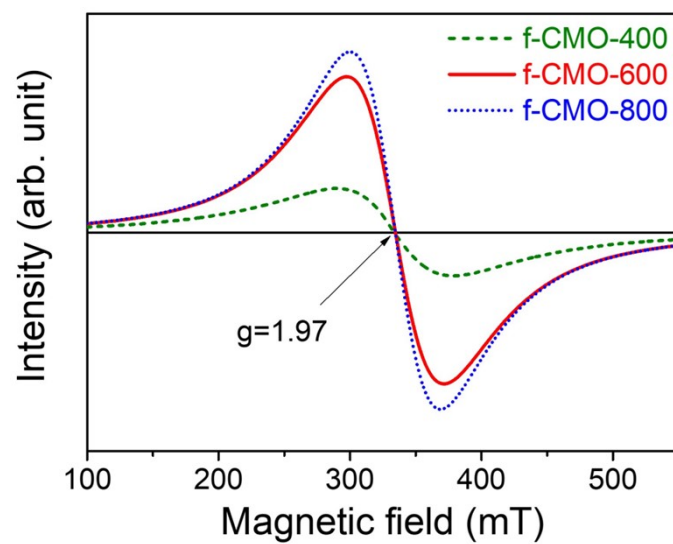
$$\text{Faradic efficiency (FE)} = \frac{\text{moles of } H_2}{J \times A \times t/n \times e \times N_A}$$

where  $J$  is the current density ( $A \text{ cm}^{-2}$ ),  $A$  is the area ( $\text{cm}^2$ ),  $t$  is the time (s),  $e$  is the elementary charge ( $1.602 \times 10^{-19} \text{ C}$ ),  $n = 2$  for  $H_2$ , and  $N_A$  is Avogadro's number ( $6.02 \times 10^{23} \text{ mol}^{-1}$ ).

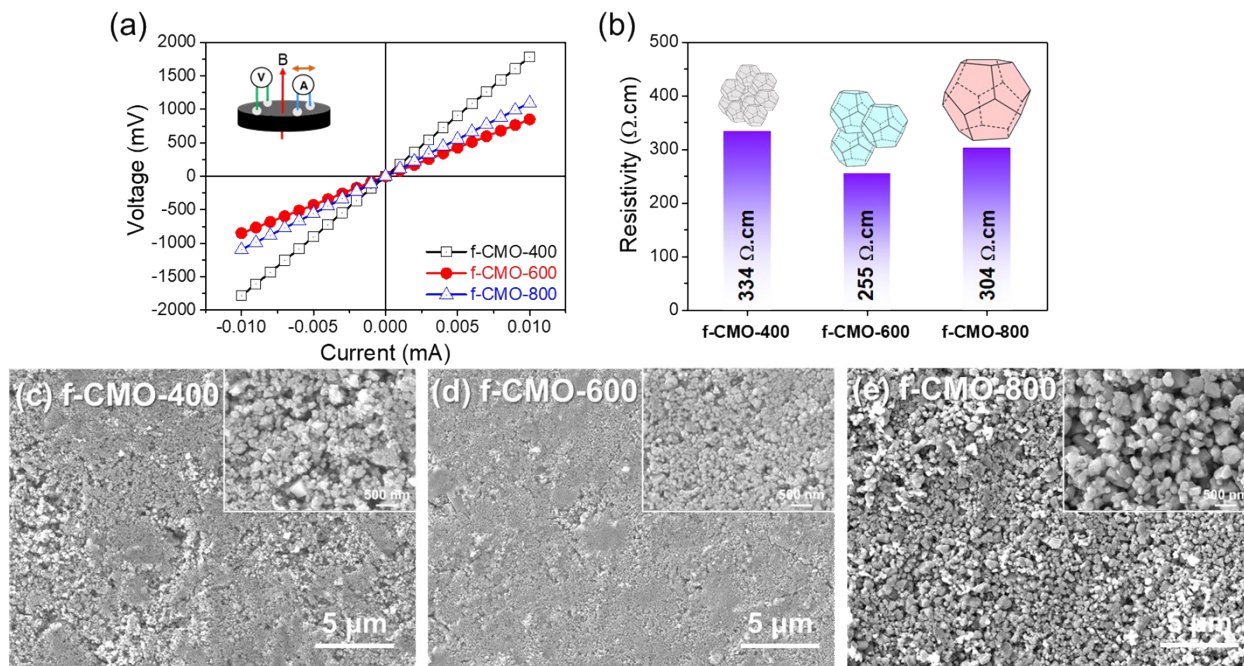




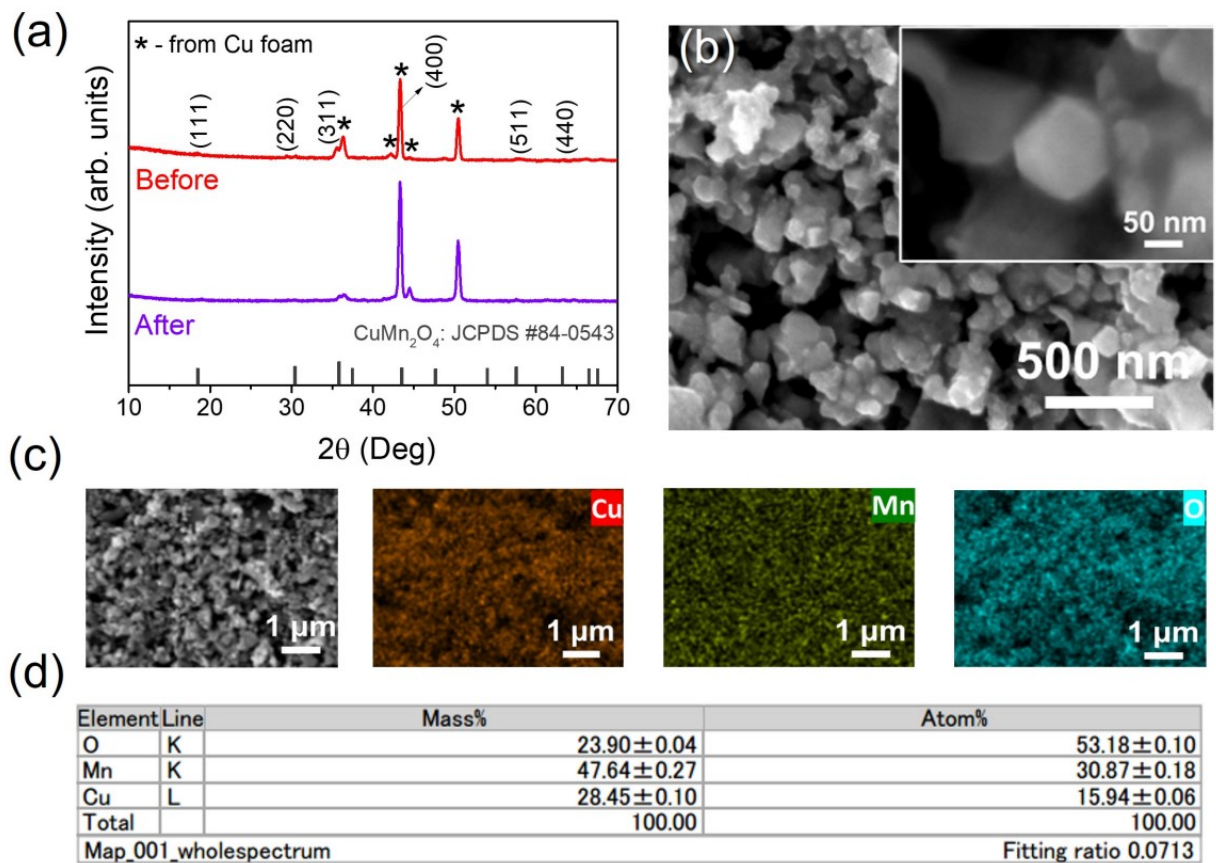
**Fig. S17. X-ray photoelectron spectroscopy (XPS) analysis of f-CMO:** Survey spectra of f-CMO-400, f-CMO-600 and f-CMO-800.



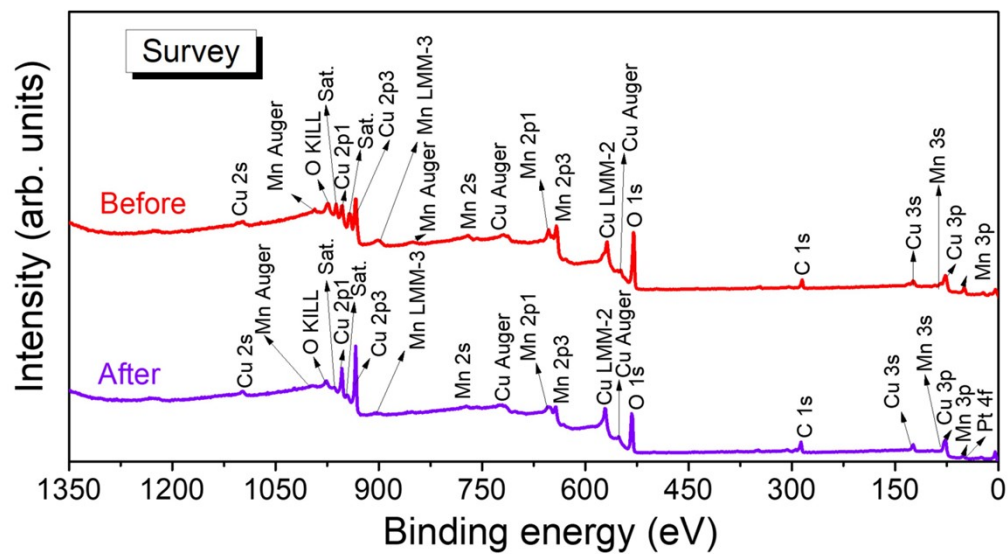
**Fig. S18. Oxygen vacancies analysis:** Electron paramagnetic resonance (EPR) spectra of f-CMO-400, f-CMO-600 and f-CMO-800.



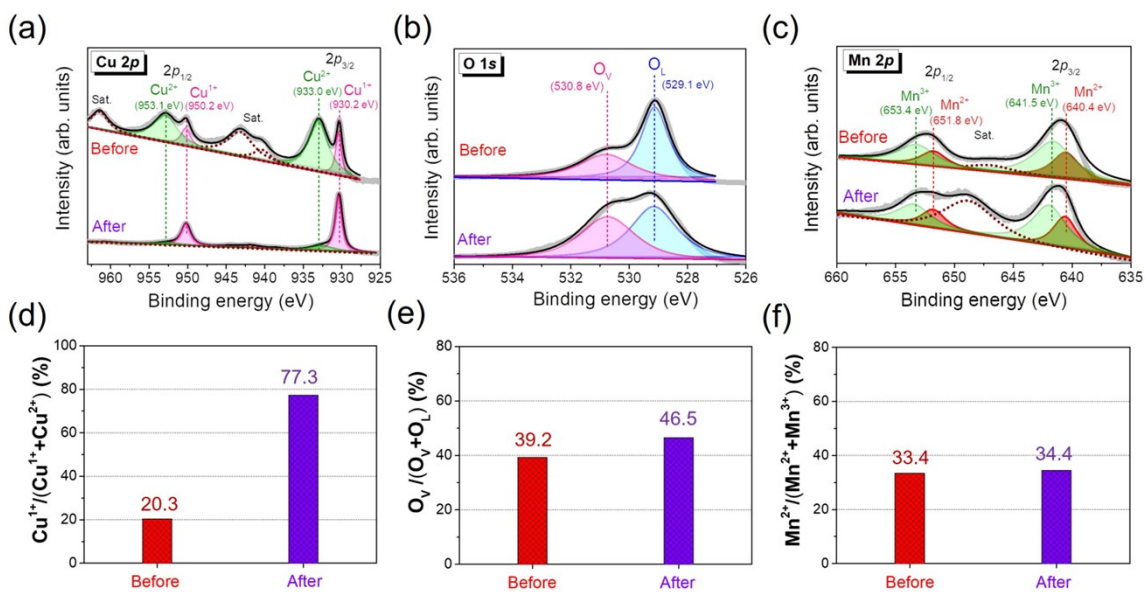
**Fig. S19. Hall voltage measurement and surface analysis of f-CMO (pellet):** (a) I–V curves in the applied static current range of -10 to 10  $\mu\text{A}$  @room temperature. (Inset image shows the schematic representation of Hall measurement circuit). (b) Comparison of room-temperature resistivity. The applied magnetic field (B) is 0.545 T. (c-e) SEM images of the pellet. (Inset image shows high magnification).



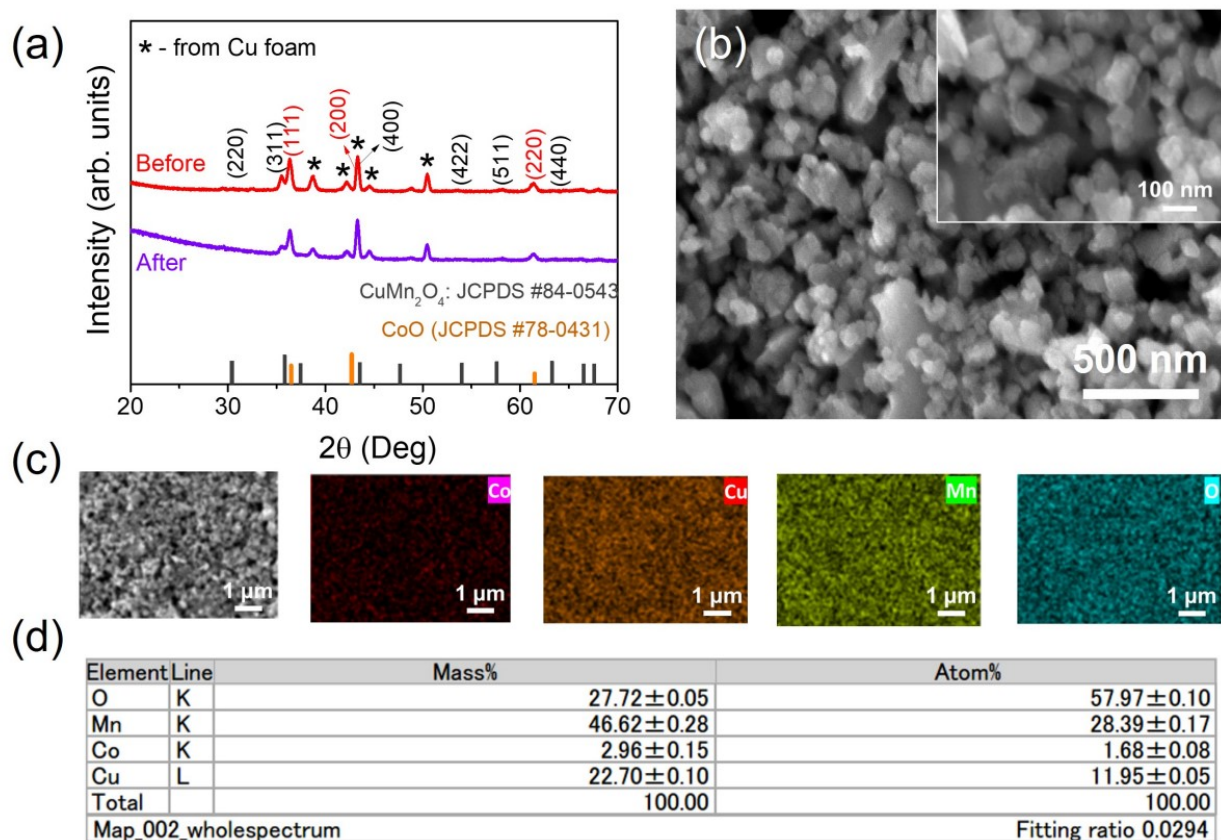
**Fig. S20. Structural and morphological analyses of f-CMO-600 electrode after 50 h of HER activity in 1 M KOH:** (a) XRD pattern. (b) SEM image. (c) SEM-EDS elemental mapping. (d) SEM-EDS microanalysis results.



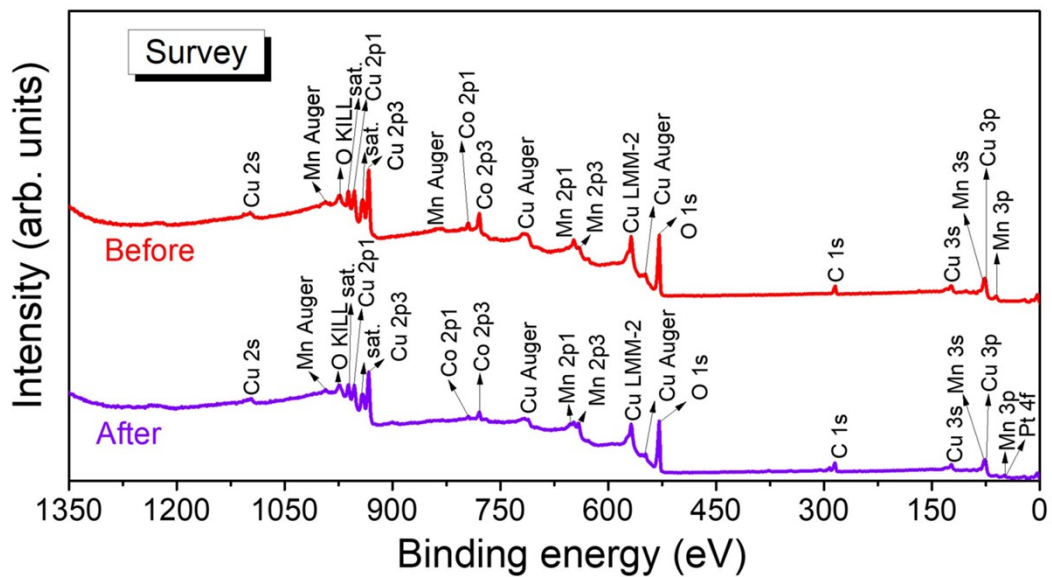
**Fig. S21.** XPS survey scan of f-CMO-600 before and after 50 h HER stability.



**Fig. S22. X-ray photoelectron spectroscopy (XPS) analysis of f-CMO-600 electrode before and after 50 h of HER activity in 1 M KOH:** High-resolution XPS spectra of (a) Cu 2p. (b) O 1s. (c) Mn 2p. The relative percentage of (d) Cu<sup>1+</sup> (from Cu 2p<sub>3/2</sub>). (e) O<sub>V</sub>. (f) Mn<sup>2+</sup> (from Mn 2p<sub>3/2</sub>).

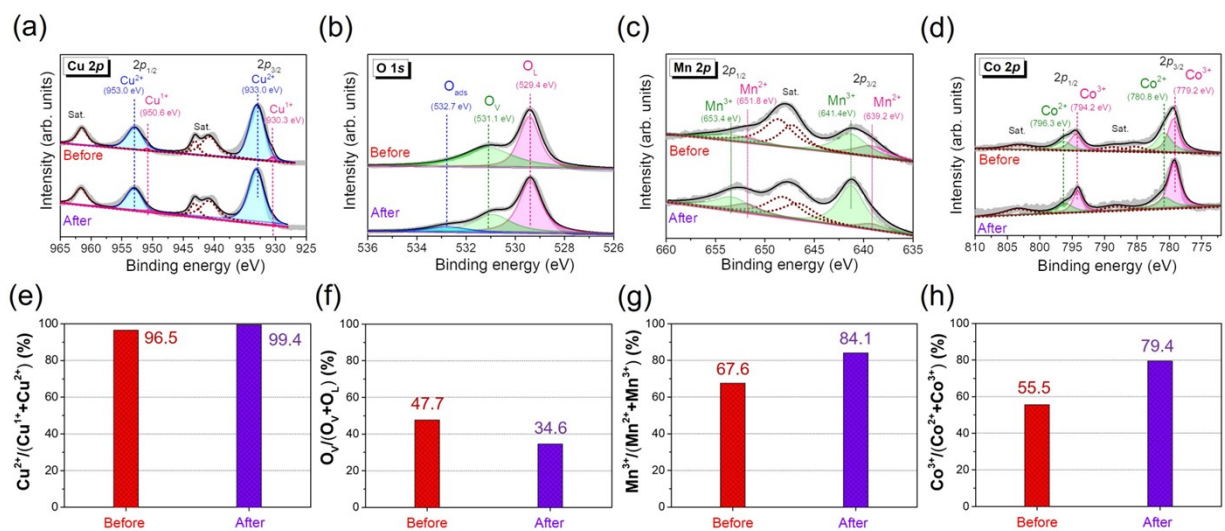


**Fig. S23. Structural and morphological analyses of  $\text{CoO}_x/\text{f-CMO-600}$  electrode after 10 h of OER activity in 1 M KOH:** (a) XRD pattern. (b) SEM image. (c) SEM-EDS elemental mapping. (d) SEM-EDS microanalysis results.

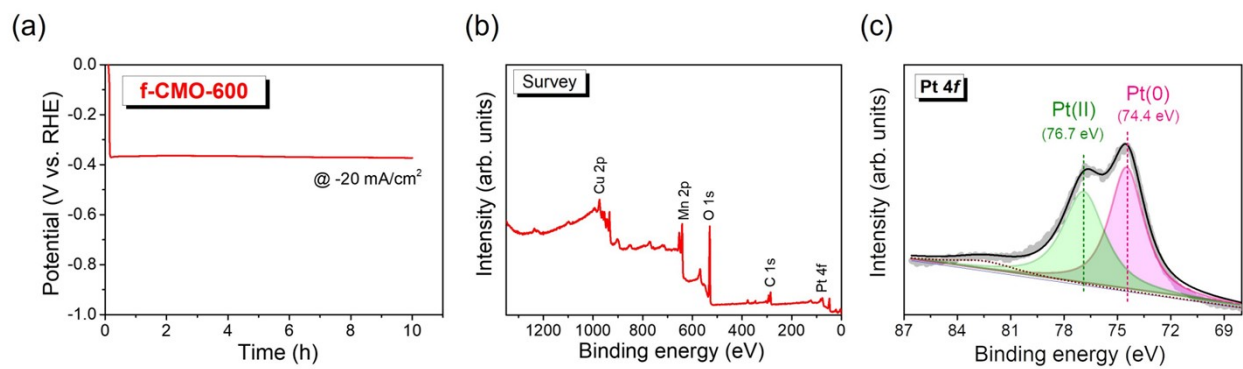


**Fig. S24.** XPS survey scan of  $\text{CoO}_x/\text{f-CMO-600}$  before and after 10 h OER stability.

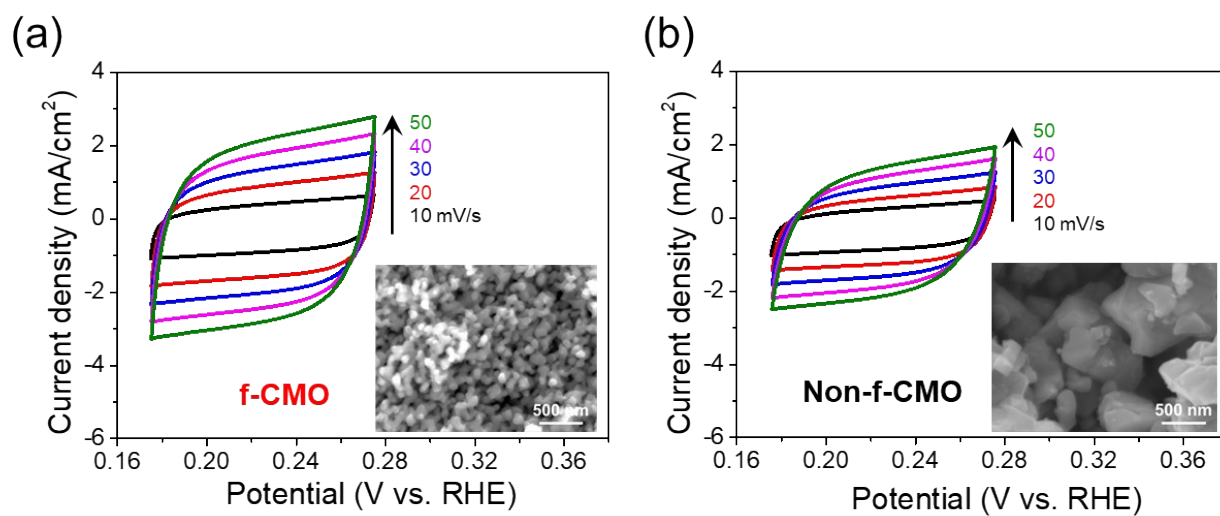




**Fig. S25. X-ray photoelectron spectroscopy (XPS) analysis of CoO<sub>x</sub>/f-CMO-600 electrode before and after 10 h of OER activity in 1 M KOH:** High-resolution XPS spectra of (a) Cu 2p. (b) O 1s. (c) Mn 2p. (d) Co 2p. The relative percentage of (e) Cu<sup>2+</sup> (from Cu 2p<sub>3/2</sub>). (f) O<sub>v</sub>. (g) Mn<sup>3+</sup> (from Mn 2p<sub>3/2</sub>). (h) Co<sup>3+</sup> (from Co 2p<sub>3/2</sub>).



**Fig. S26.** (a) Chronopotentiometry (CP) of f-CMO-600 at  $-20 \text{ mA/cm}^2$  for 10 h. (b) XPS survey scan after CP test. (c) High-resolution XPS spectrum of Pt 4f.



**Fig. S27. Impact of facets on the electrochemical active surface area (ECSA) of CMO:** Cyclic voltammograms (CVs) of (a) f-CMO. (b) Non-f-CMO at different scan rates (10, 20, 30, 40 and 50 mV/s).